INTERNATIONAL JOURNAL OF
NUMERICAL ANALYSIS AND MODELING
Volume 22, Number 1, Pages 21–39

doi: 10.4208/ijnam2025-1002

IMAGE SMOOTHING VIA A NOVEL ADAPTIVE WEIGHTED L_0 REGULARIZATION

WUFAN ZHAO, TINGTING WU, CHENCHEN FENG, WENNA WU, XIAOGUANG LV, HONGMING CHEN, AND JUN LIU*

Abstract. Image smoothing has been extensively used in various fields, e.g., edge extraction, image abstraction, and image detail enhancement. Many existing optimization-based image smoothing methods have been proposed in recent years. The downside of these methods is that the results often have unclear edges and missing structures. To obtain satisfactory smoothing results, we design a novel optimization model by introducing an anisotropic L_0 gradient intensity. Specifically, a weighted matrix $\mathbf{T}$ is imposed to control further the sparsity of the gradient measured by L_0-norm. Since the proposed model is non-convex and non-smooth, we apply the half quadratic splitting (HQS) algorithm to solve it effectively. In addition, to obtain a more suitable regularization parameter λ, we utilize an adaptive parameter selection method based on Morozovs discrepancy principle. Finally, we conduct numerical experiments to illustrate the superiority of our method over some state-of-the-art methods.

Key words. Image smoothing, adaptive weighted matrix, L_0 gradient minimization, parameter selection.

1. Introduction

Image smoothing has a broad variety of applications as basic visual research, such as image detail enhancement [8], edge extraction [41], clip-art compression artifact removal [39, 32], image denoising [15, 31, 37], image segmentation [30, 33] and image abstraction [38]. Image smoothing aims to obtain an image with complete structural content but without small textures, which is undoubtedly challenging. Actually, many advanced image smoothing algorithms have been studied over recent years [4, 46, 22].

Model-based methods have been paid much attention because of their excellent performance and solid theoretical guarantee. The optimization model related to image smoothing is usually written as

$$\min_u \|u - f\|_2^2 + \lambda\varphi(u), \tag{1}$$

where f and u denote the input image and the resulting smoothed image, respectively. λ is a tradeoff parameter used to adjust the degree of regularization. Many methods are devoted to selecting an appropriate regularizer to smooth the image more effectively. Xu *et al.* [39] used L_0-norm to remove a globally small-magnitude gradient with edge preservation. However, this method failed to deal with small structures with large amplitude and small resolution. The relative total variation (RTV) [41] based regularization is employed to extract main structures under the complex texture. Liu *et al.* [20] combined the L_0 sparse constraint with the nonlocal constraint to remove the fine texture of the image. However, the above methods

Received by the editors on September 18, 2023 and, accepted on September 1, 2024.
2000 *Mathematics Subject Classification.* 65D18, 68U10, 94A08.
*Corresponding author.

are not flexible enough in gradient processing, which hinders their ability to protect weak edges and eliminate fine textures effectively. In Figure 1(b), we show the limitation of the L_0 smoothing.

(a) Input (b) L_0 [39] (c) Ours

FIGURE 1. An example of L_0 smoothing [39] and our method. The result of [39] can not remove small structures. In contrast, our method achieves a more convincing result.

Total variation (TV) regularization is also capable of smoothing. However, it tends to lose local structure and produce artifacts. To cope with this barrier, many previous works that combine anisotropic filtering with TV regularization have been proposed [25, 43]. In [26], the authors employ the characteristics of anisotropic total variation (ATV) to remove noise while retaining the complete structure:

$$\min_u \|u - f\|_2^2 + \lambda \|\mathbf{T}\nabla u\|_1, \tag{2}$$

where $\mathbf{T}(x, y) := \mathrm{diag}(t_1(x, y), t_2(x, y))$ and (x, y) denotes the pixel location of u. For each pixel, the gradient of the image $\nabla u = (\nabla_x u, \nabla_y u)$ is the difference of adjacent pixels along the x-axis and y-axis. In fact, $\mathbf{T}(x, y)$ can impose different penalty weights on $\nabla_x u(x, y)$ and $\nabla_y u(x, y)$. In this work, we try to introduce the weighted matrix $\mathbf{T}(x, y)$ into our smoothing model, i.e., we combine anisotropic filtering with L_0 smoothing. The proposed adaptive weighted L_0 regularization model is as follows:

$$\min_u \|u - f\|_2^2 + \lambda \|\mathbf{T}\nabla u\|_0, \tag{3}$$

where $\|\cdot\|_0$ denotes the L_0-norm and λ is the regularization parameter. This regularization term can flexibly handle gradients and depict local details of images, such as weak edges and small structures. As is well known, the parameter λ also has an impact on the image smoothing effect. A large λ can cause the image to be too smooth and weak edges to disappear, while a small λ cannot remove unrelated textures that exist in the image. A good optimization model should have an appropriate regularization parameter. Common parameter adjustment methods include the L-curve-based approach [18], the generalized cross-validation method [10], the variational Bayesian method [1], and Morozovs discrepancy principle [34, 24]. Specifically, Morozovs discrepancy principle is one of the most widely used

parameter choice strategies, where a regularization parameter with the following conditions:

$$D = \{u : \|Au - f\|_2^2 \leq c^2\}, \tag{4}$$

with $c^2 = \tau n_1 n_2 \sigma^2$, σ^2 is the unknown noise variance, τ is usually set to be 1 and A is a degenerate operator. Using this criterion, the problem of model parameter selection is transformed into the problem of noise estimation, which makes the problem easy to solve. Here, we can use the median rule [23] to estimate the unknown noise variance σ^2. In our image smoothing model, the degenerate operator A is an identity matrix.

In a nutshell, the primary contribution of this novel strategy can be summarized as follows:

(1) We present a novel L_0 regularization image smoothing model that uses the weighted matrix $\mathbf{T}$ to better characterize the local structure of the smoothing results.
(2) To deal with the weight relationship between the fitting term and the regularization term, we design a parameter adaptive method to estimate the regularization parameter λ using Morozovs discrepancy principle.
(3) Extensive experiments conducted on different tasks validate the excellent performance of the designed scheme.

The outline of our paper is organized as follows: Section 2 briefly reviews the relevant image smoothing methods. A detailed presentation of our model is presented in Section 3. Comprehensive experimental results are given to show the superior performance of our method in Section 4. Finally, Section 5 provides conclusions.

2. Related Work

Massive image smoothing technologies have been proposed in the past few decades, which can be roughly divided into filter-based methods, optimization-based methods, and learning-based methods.

2.1. Filter-based methods. The method based on filters is mainly to carry out the weighted average for each pixel and its adjacent pixels. Guided filtering (GF) [13] is a typical kind of such method, which can avoid gradient inversion artifacts. The rolling guidance filter (RGF) [44] effectively solved the problem of contour and boundary loss in the composition of smoothing texture by other filters. The SD filter [12] considered the structural differences between the guide image and the input image, and processed different types of data under a unified framework. Although GF has low computational complexity and inspires other methods, it will cause edge blur. Cho *et al.* designed a bilateral filter [5] to protect the edges of the image which became a typical representative of such methods. Laplace filter [27] used the Laplace pyramid to decompose the image at multiple scales to obtain edge information. Karacan *et al.* [17] adopted the region covariance matrix to indirectly extract texture information and local structure to highlight edges and shadows, and improved the applicability of other applications. Based on the segment graph, Zhang *et al.* [42] introduced a double weighted average filter to overcome the halo artifacts in applications.

2.2. Optimization-based methods. Optimization-based image smoothing methods are also representative approaches in image processing. Xu *et al.* [39] used the L_0-norm to remove a globally small-magnitude gradient with edge preservation.

However, this method cannot handle structures with large amplitude and small resolution. Then, Xu *et al.* [41] developed an RTV-based optimization model and used it to extract main structures and remove textures. Later, an L_0 gradient minimization method based on the region fusion [28] is proposed to solve the minimization problem quickly and effectively while improving the smoothing effect. He *et al.* designed a truncated L_0 gradient regularization [15], which has an obvious sharpening effect on the critical edge. Wen *et al.* [35] used two different norms to decompose images: TV-norm to capture the cartoon component, and G-norm to capture the texture component. The bilateral total variation (BTV) [16] was introduced in the past to distinguish between structure and texture, and identify local structures and weak edges simultaneously. The scheme also adopted a multi-scale awareness strategy to enhance the ability of the regularization to protect small structures. Liu *et al.* [21] proposed a generalized framework for edge or structure preserving (GFES), which adapts to different applications by adjusting different parameter settings of the truncated Huber penalty function. Zhu *et al.* [46] gave three non-convex penalty functions, all of which can be used as regularization terms for image smoothing. This method shows effectiveness in various image processing tasks. Li *et al.* [19] proposed an image smoothing method based on truncating the generalized Huber prior (TGHF). The method applies to a wide range of image smoothing problems and is good at preserving edges and structure while maintaining color contrast. However, the above methods have poor processing of weak edges, leading to unclear edges of the smoothed image. The primary cause is that these variational methods are not flexible enough to deal with gradients, making it difficult to accurately distinguish texture and structure.

2.3. Learning-based methods. Lately, the emergence of deep learning has greatly developed image smoothing algorithms [40, 7, 45, 38, 9]. Some methods are devoted to designing new datasets and applying the convolutional network to them for training. Then they can obtain satisfactory image smoothing effects [45, 38, 9]. Chen *et al.* [3] used a full convolution neural network to describe the global attributes of images. In [45], the author adopted VDCNN [6] and ResNet [14] as the baseline methods and designed a loss function suitable for edge smoothing. However, the results of these methods mostly depend on the dataset and are generally not good on other wild data. Fan *et al.* [7] proposed an unsupervised learning method, which helps maintain fragile edges and structures by designing new energy functions. This method applies different regularizations to different regions by a spatially adaptive L_p flattening standard. In contrast, the learning-based methods are more time-consuming and computationally complex during the training period.

3. Model and Algorithm

In this section, we propose a weighted adaptive L_0 regularization method. Then we utilize the half quadratic splitting [11] algorithm to solve the proposed optimization model. By flexibly adjusting the adaptive weight matrix $\mathbf{T}$, a satisfactory smoothed image is obtained. We also design a parameter adaptation scheme suitable for our model to generate an appropriate regularization parameter.

3.1. Adaptive weighted matrix. There are many approaches to extracting the structural features of images using the anisotropic TV [2, 36]. Especially, it is important to select a suitable weighted matrix $\mathbf{T}$ for the anisotropic TV. In this paper, inspired by [26], the adaptive weighted matrix is defined as:

$$\begin{aligned}\mathbf{T}(x,y) &= \begin{bmatrix} t_1(x,y) & 0 \\ 0 & t_2(x,y) \end{bmatrix} \\ &= \begin{bmatrix} \frac{1}{1+\kappa|G_\sigma(x,y)*\nabla_x u(x,y)|^2} & 0 \\ 0 & \frac{1}{1+\kappa|G_\sigma(x,y)*\nabla_y u(x,y)|^2} \end{bmatrix},\end{aligned} \tag{5}$$

where κ and σ are positive parameters, $*$ denotes the convolution operator. And the Gaussian kernel is defined as $G_\sigma(x,y) = \frac{1}{2\pi\sigma^2}\exp(-\frac{\|x\|^2+\|y\|^2}{2\sigma^2})$. When $t_1(x,y)$ and $t_2(x,y)$ take two equal constants, our model tends to be the model proposed by Xu *et al.* [39]. The corresponding gradient is isotropic. Coupling the matrix $\mathbf{T}(x,y)$ and the gradient $\nabla u(x,y)$ together is rotating $\nabla u(x,y)$ with an angle of $\alpha-\beta$. As shown in Figure 2 (b), when $|t_1(x,y)u_x(x,y)| < |t_2(x,y)u_y(x,y)|$, the horizontal direction will have greater weight. In this way, our method can obtain the overall structure of the image more effectively when a suitable $\mathbf{T}(x,y)$ is selected.

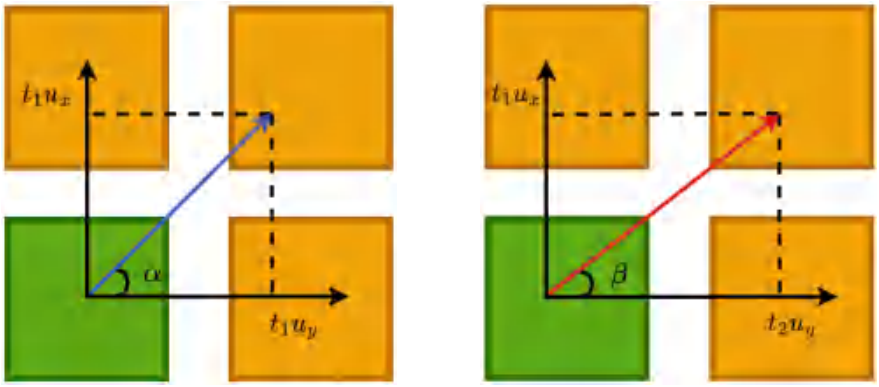

(a) Isotropic gradient (b) Anisotropic gradient

FIGURE 2. The $\nabla u(x,y)$ with the adaptive weighted matrix $\mathbf{T}(x,y)$: $|t_1(x,y)u_x(x.y)| < |t_2(x,y)u_y(x,y)|$. And we set $\alpha = \arctan\frac{\nabla_y u(x,y)}{\nabla_x u(x,y)}$ and $\beta = \arctan(\frac{t_2(x,y)\nabla_y u(x,y)}{t_1(x,y)\nabla_x u(x,y)})$.

3.2. Algorithm. Here, we utilize the HQS algorithm to solve Eq. (3) by separating operators $\mathbf{T}$ and ∇ from L_0-norm. The constrained minimization problem can be written as:

$$\begin{aligned}&\min_{u,\mathbf{w},\mathbf{v}} \|u-f\|_2^2 + \lambda\|\mathbf{w}\|_0, \\ &\text{s.t.}\mathbf{w} := (w_1,w_2)^T = \mathbf{T}\mathbf{v}, \mathbf{v} := (v_1,v_2)^T = \nabla u.\end{aligned} \tag{6}$$

After introducing auxiliary variable $\mathbf{w}$ and $\mathbf{v}$, we rewrite the above problem as:

$$\min_{u,\mathbf{w},\mathbf{v}} \|u-f\|_2^2 + \lambda\|\mathbf{w}\|_0 + \eta\|\mathbf{w}-\mathbf{T}\mathbf{v}\|_2^2 + \omega\|\mathbf{v}-\nabla u\|_2^2, \tag{7}$$

where ω, η are positive penalty parameters.

3.2.1. u-subproblem. Collecting the u-involved terms from Eq. (7), we have the following optimization problem:

$$\min_{u} \|u - f\|_2^2 + \omega \|\mathbf{v} - \nabla u\|_2^2 . \tag{8}$$

When the periodic boundary conditions are applied to the gradient, we can tackle this minimization problem effectively by using fast Fourier transform (FFT) and inverse fast Fourier transform (IFFT):

$$u = \mathcal{F}^{-1}\left(\frac{\mathcal{F}(f) + \omega(\mathcal{F}^*(\nabla_x)\mathcal{F}(v_1) + \mathcal{F}^*(\nabla_y)\mathcal{F}(v_2))}{\mathcal{F}(I) + \omega(\mathcal{F}^*(\nabla_x)\mathcal{F}(\nabla_x) + \mathcal{F}^*(\nabla_y)\mathcal{F}(\nabla_y))}\right), \tag{9}$$

where $\mathcal{F}$ denotes the FFT operator.

3.2.2. w-subproblem. The $\mathbf{w}$-subproblem is a classical L_0 problem:

$$\min_{\mathbf{w}} \|\mathbf{w} - \mathbf{T}\mathbf{v}\|_2^2 + \frac{\lambda}{\eta} \|\mathbf{w}\|_0 . \tag{10}$$

It can be solved by hard thresholding:

$$(w_1, w_2) = \begin{cases} (0,0), & (t_1 v_1)^2 + (t_2 v_2)^2 \le \lambda/\eta, \\ (t_1 v_1, t_2 v_2), & \text{otherwise.} \end{cases} \tag{11}$$

3.2.3. v-subproblem. We collect terms about $\mathbf{v}$ as follows:

$$\min_{\mathbf{v}} \eta \|\mathbf{w} - \mathbf{T}\mathbf{v}\|_2^2 + \omega \|\mathbf{v} - \nabla u\|_2^2. \tag{12}$$

With a simple computation, we can obtain

$$\begin{aligned} v_1 &= \frac{\eta t_1 w_1 + \omega \nabla_x u}{\omega + t_1^2}, \\ v_2 &= \frac{\eta t_2 w_2 + \omega \nabla_y u}{\omega + t_2^2}. \end{aligned} \tag{13}$$

Finally, we update η by $\eta := \rho \cdot \eta$ and stop iteration until $\eta < \eta_{max}$. The whole process of our algorithm is shown in Algorithm 1.

Algorithm 1 Image Smoothing via the adaptive weighted L_0 gradient intensity

1: The input image f, $u^{(0)} = f$, $k = 0$, parameter λ, η, ω, κ, σ, η_{max}, ρ;
2: **while** not converged **do**
3: Update $u^{(k)}$ via Eq. (9);
4: Update $\mathbf{w}^{(k+1)}$ via Eq. (11);
5: Update $\mathbf{v}^{(k+1)}$ via Eq. (13);
6: **end while**
7: The smoothed image u.

3.3. Parameter Adaptation. For the selection of parameter λ, a manual trial-and-error method is usually time-consuming and tedious. Based on this consideration, we introduce Morozovs discrepancy principle strategy into the new model to adaptively generate an appropriate regularization parameter during the iteration. The proposed parameter selection method effectively balances the regularization term and the fitting term. For convenience, Eq. (3) can be rewritten as follows:

$$\min_{u,\gamma} \gamma \|u - f\|_2^2 + \|\mathbf{T}\nabla u\|_0 , \tag{14}$$

here, we set $\gamma = \frac{1}{\lambda}$. Accordingly, $u-$subproblem can be modified as follows:

$$u_\gamma = (\gamma I + \omega \nabla^T \nabla)^{-1}(\gamma f + \omega \nabla^T \mathbf{v}). \tag{15}$$

Based on Morozovs discrepancy principle, we can analyze discrepancy e_γ given by

$$\begin{aligned} e_\gamma &= u_\gamma - f \\ &= (\gamma I + \omega \nabla^T \nabla)^{-1}(\gamma f + \eta \nabla^T \mathbf{v}) - f \\ &= (\gamma I + \omega \nabla^T \nabla)^{-1}(\omega \nabla^T \mathbf{v} + \omega \nabla^T \nabla f). \end{aligned} \tag{16}$$

Let $\Phi(\gamma, \mathbf{v}) = \|e_\gamma\|_2^2$ and $D_\gamma = \{u : \|u_\gamma - f\|_2^2 \leq c^2\}$, according to [34], when $\|u_{\gamma_k}^{(k)} - f\|_2^2 > c^2$, the equation $\Phi(\gamma_k, \mathbf{v}^{(k-1)}) = c^2$ has a unique solution. This means that we can find a unique $\gamma_k > 0$ when $u_{\gamma_k}^{(k)} \notin D$ that meets $\|u_{\gamma_k}^{(k)} - f\|_2^2 = c^2$. And $\gamma_k = 0$ when $u^{(k)} \in D$. It should be noted that the equation $\Phi(\gamma^{(k)}, \mathbf{v}^{(k-1)}) = c^2$ is nonlinear and can be solved iteratively by the Newton method. Algorithm 2 summarizes the whole process of the strategy.

Algorithm 2 Image Smoothing via the adaptive weighted L_0 gradient intensity and the adaptive parameter selection

```
The input image f, u^(0) = f, k = 0, parameter λ, η, ω, κ, σ, η_max, ρ;
while not converged do
    Update u^(k) via Eq. (15);
    Update w^(k+1) via Eq. (11);
    if u^(k) ∈ D then
        γ_k = 0;
    else
        Solve Φ(γ, v) = c^2 for γ_k;
    end if
    Update v^(k+1) via Eq. (13);
end while
The smoothed image u.
```

4. Experimental Results

To verify the effectiveness of our model, we compare it with the well-known methods both qualitatively and quantitatively: L_0 [39], RTV [41], RGF [44], Pixel-level Non-Local Smoothing (PNLS) [38], GFES [21], Scale-adaptive Structure-preserving Texture Filtering (SSTF) [29], G-norm [35], SD filter [12], TGHF[19], Nonconvex Regularization for Convex Image Smoothing (NRCS) [46]. In addition, we also expand our model to some related applications such as image detail enhancement, edge extraction, clip-art compression artifact removal, image denoising, and image abstraction. All experiments are run on MATLAB 2019b and the parameters of the methods for comparison are set as recommended.

4.1. Image Smoothing.

4.1.1. Subjective visual results. Image smoothing aims to remove unrelated textures while preserving the edges of the image. Our method can achieve an impressive smooth performance with the adaptive weight matrix. We test the following types of images: (1) The image with small textures that need to be smoothed, as shown in Figure 3(a). (2) Obvious textures in the image should be smoothed while protecting weak edges, as shown in Figure 4(a). The mouth labeled

with the green arrow in the red box of Figure 4(a) indicates the existing weak edges. (3) Figure 5(a) is an image containing multi-scale textures, that requires the removal of large textures while retaining the underlying structure.

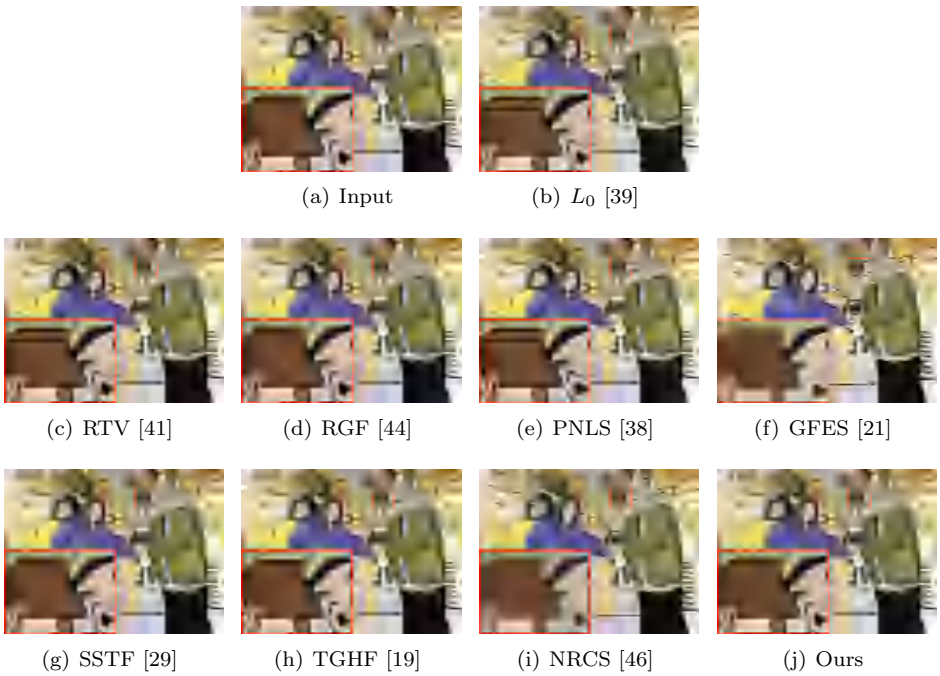

(a) Input (b) L_0 [39]

(c) RTV [41] (d) RGF [44] (e) PNLS [38] (f) GFES [21]

(g) SSTF [29] (h) TGHF [19] (i) NRCS [46] (j) Ours

FIGURE 3. The smoothing results of several state-of-the-art methods. For each smoothed result, the zoomed-in patches of the smoothed output are shown in the bottom left.

As presented in Figure 3(a), small textures in the image need to be smoothed without removing strong edges. The results obtained by L_0, RTV, and TGHF have obvious texture residues, as shown in Figure 3(b), (c), (h). While PNLS and RGF fail to remove the texture in Figure 3(e) and (f). Although GFES, SSTF, and NRCS smooth the texture to some extent, they over-blur the structural edges as shown in Figure 3(f), (g), and (i). On the contrary, our result shows high-quality performance: the texture in small areas is eliminated, and the overall structure is maintained.

Figure 4(a) demonstrates a complex image with weak edges and multi-scale features, which implies that we need to smooth large textures while extracting small structures. The results of the L_0 and TGHF methods have many obvious textures, although they extract some meaningful structures. The RTV, GFES, and NRCS methods reliably remove large textures, however, they fail to maintain the weak edges. Similarly, RGF, PNLS, and SSTF can remove the obvious textures well, but the edges of the highlighted regions are blurred. As for our method, we have a meticulous treatment in extracting weak edges (the red box of Figure 4(h)) and removing large textures (the green box of Figure 4(h)) by using the novel regularization we design. Our result demonstrates superior smoothing performance with clear boundaries.

(a) Input (b) L_0 [39]

(c) RTV [41] (d) RGF [44] (e) PNLS [38] (f) GFES [21]

(g) SSTF [29] (h) TGHF [19] (i) NRCS [46] (j) Ours

FIGURE 4. The smoothing results of several state-of-the-art methods. For each smoothed result, the zoomed-in patches of the smoothed output are shown on the right.

Figure 5(a) shows a typical image with multi-scale textures. An ideal smoothing result would be to remove large textures while maintaining small structures. In Figure 5, we can easily notice that L_0, RTV, PNLS, TGHF, and NRCS methods are unsatisfactory for removing large textures because the results still contain many white blocks. RGF and SSTF produce blurry edges and an unsmoothed background. Although the GFES method performs well in the enlarged green area, it yields poor smoothing results in the gray background. From Figure 5(h), it is evident that our method performs well in both large texture removal and background smoothing. Overall, our method can achieve the best visual effect in image smoothing.

4.1.2. Objective numerical results. We further conduct a quantitative comparison to ensure the persuasiveness of the experiment. Especially, we adopt two 256×256 cartoon images [35] with different textures (as shown in Figure 6). Table 1 reports the PSNR of three methods under different synthetic images. Our method outperforms G-norm, L_0, TGHF, and NRCS methods in 7 images, clearly demonstrating its superiority.

4.1.3. A/B testing of the dataset. Xu *et al.* [41] collected 200 structural texture images and drew images of important structural edges for each image, resulting

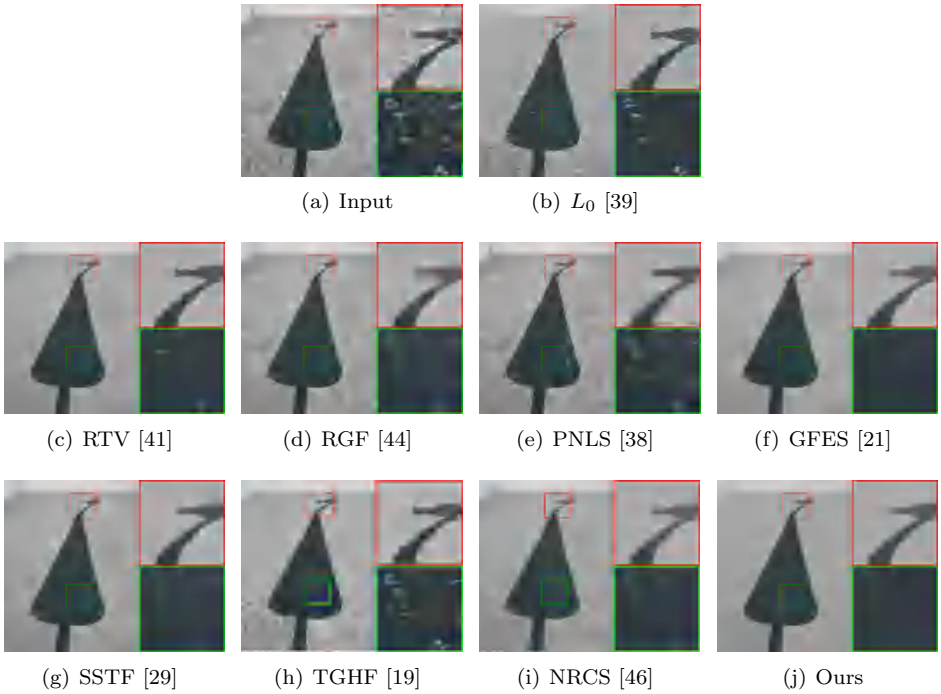

(a) Input (b) L_0 [39]

(c) RTV [41] (d) RGF [44] (e) PNLS [38] (f) GFES [21]

(g) SSTF [29] (h) TGHF [19] (i) NRCS [46] (j) Ours

FIGURE 5. The smoothing results of several state-of-the-art methods. For each smoothed result, the zoomed-in patches of the smoothed output are shown on the right.

TABLE 1. Quantitative comparison results (PSNR) of several methods on synthetic images.

Image	Textures	G-norm [35]	L_0 [39]	NRCS [46]	TGHF [19]	Ours
Ball	35a8c	34.56	34.18	32.74	31.28	**34.63**
	4bada	31.99	32.70	32.78	31.19	**34.81**
	brickrg	30.86	32.54	32.32	29.50	**33.72**
	weave	32.91	34.75	32.45	30.53	**35.93**
	Ave.	32.58	33.54	32.57	30.63	**34.77**
Mixedpic	35a8c	**35.54**	32.07	32.24	31.50	34.95
	4bada	32.26	30.44	31.69	31.02	**32.74**
	brickrg	31.25	30.38	32.05	29.99	**31.86**
	weave	33.91	32.13	32.19	31.65	**34.72**
	Ave.	33.24	31.25	32.04	31.04	**33.56**

in a total of 400 images that were used to form a dataset[1]. The source images of Figure 5, Figure 9 and Figure 14 in this paper are from this dataset.

Given that individuals perceive details and major structures in disparate ways, they may hold disparate preferences regarding the optimal image smoothing result. To address this, we recruited 20 volunteers to form a non-expert scoring panel.

[1]https://www.cse.cuhk.edu.hk/ leojia/projects/texturesep/database.html

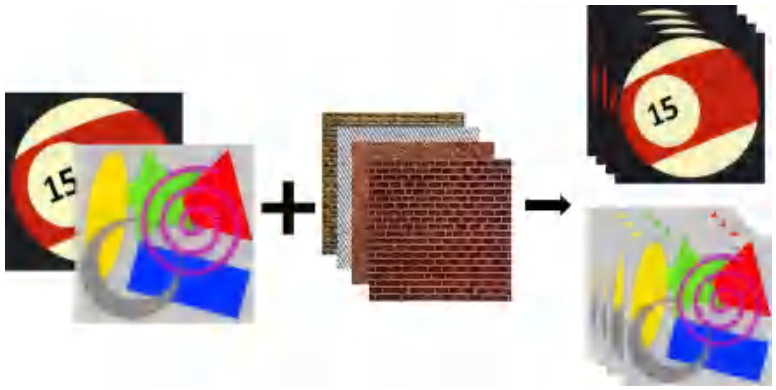

FIGURE 6. Two 256×256 synthetic images with different textures.

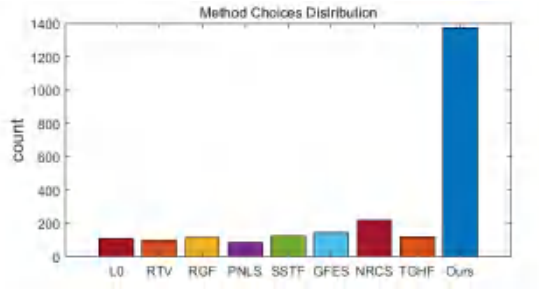

FIGURE 7. Distribution of choices between different algorithms.

These volunteers were all graduate students at Nanjing University of Posts and Telecommunications, with the majority having no prior experience in the field of image smoothing. A total of 200 structural texture images were selected from the dataset of Xu *et al.* [41]. Then, nine different image smoothing methods were applied to each source image. After a clear and concise introduction to the task, the volunteers were asked to choose the best smoothing result based on the following basic principles: retain the sharpness of critical edges, minimize blurring effects, and ensure that the color of the smoothed image is as close as possible to that of the original image.

Each source image and its corresponding smoothing result was randomly assigned to 12 volunteers, and each volunteer was allocated 120 source images and their corresponding smoothing results. Since each image was selected by 12 volunteers, there were a total of 2400 selections for these 200 source images. The results are shown in Figure 7, where 1371 selections are generated by our method. This shows that our method is effective in image smoothing.

4.2. Applications. Subsequently, we showcase several typical applications of our method, including image detail enhancement, edge extraction, clip-art compression artifact removal, image denoising, and image abstraction. All details are shown below.

4.2.1. Image Detail Enhancement. The purpose of this task is to enhance the details of the image while avoiding common halo artifacts. This task decomposes the image into two layers: a base layer and a detail layer. The enlarged detail

layer and the base layer are coupled to obtain a detail-enhanced image. Here, we subtract our model from the observed image to obtain the smooth structure to obtain the detail layer. Since the GFES method has a great effect on detail enhancement applications, we chose it for comparison. Figure 8 illustrates the results of image detail enhancement. Visually, our method produces satisfactory enhancement results and avoids the generation of halo artifacts. In addition, we can see from the 1-D plot of the highlight region that our method has both smoother results (the red line in Figure 8(e)) and more prominent enhancement effects (the blue line in Figure 8(e)). And our method is significantly better than the advanced methods compared (see details in Figures. 8(b) and (d)).

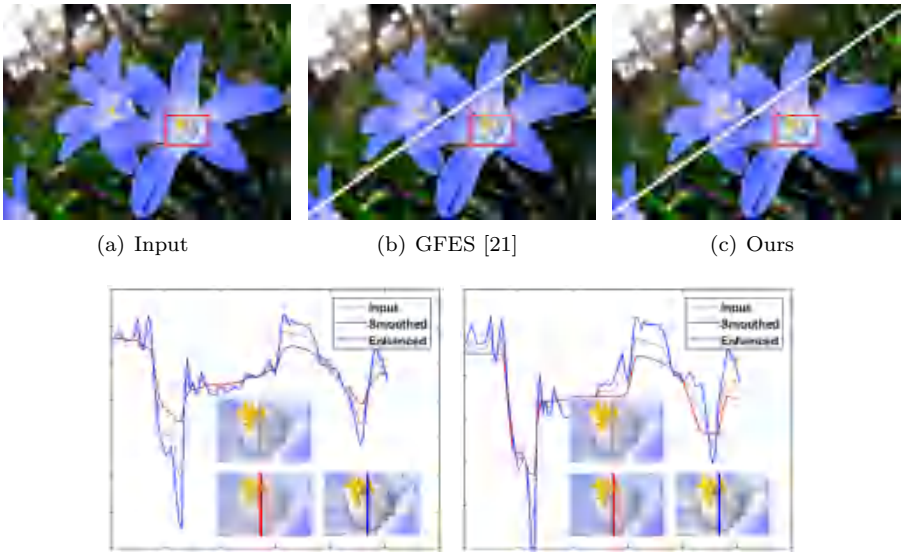

(a) Input (b) GFES [21] (c) Ours

(d) GFES [21] (e) Ours

FIGURE 8. Visual results of image detail enhancement with different approaches. (a) Input. The smoothed/enhanced results of (b) GFES [38] and (c) our method. (d) and (e) is the 1-D plot of the highlight regions.

4.2.2. Edge extraction. Generally, because natural images usually contain many textures and unexpected noises, it is difficult to achieve high accuracy by directly detecting their edges. Therefore, image smoothing can also be used as a useful tool for accurate texture image edge detection. Before the edge detection, the structure edge of the image can be directly extracted by smoothing the image. Here, we choose the model L_0 [39] and SD filter [12] which are commonly used for edge detection for quantitative and quantitative comparison.

We use a confusion matrix for quantitative comparison, mainly the measurement of $Precision$, $Recall$, $F\text{-}score$:

$$\begin{aligned} &Precision = TP/(TP + FP), \\ &Recall = TP/(TP + FN), \\ &F\text{-}score = 2Precision \cdot Recall/(Precision + Recall), \end{aligned} \tag{17}$$

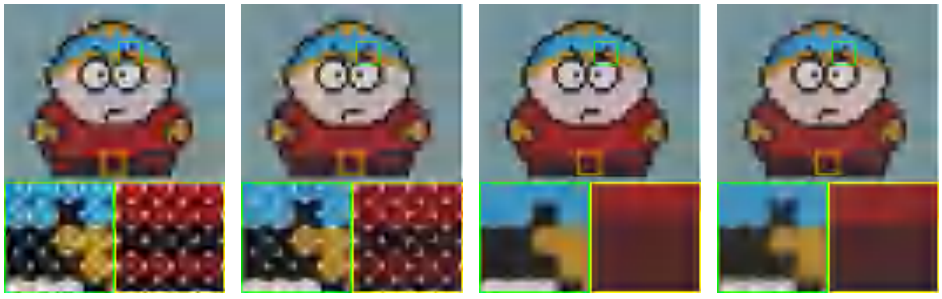

(a) Input (b) L_0 [39] (c) SD filter [12] (d) Ours

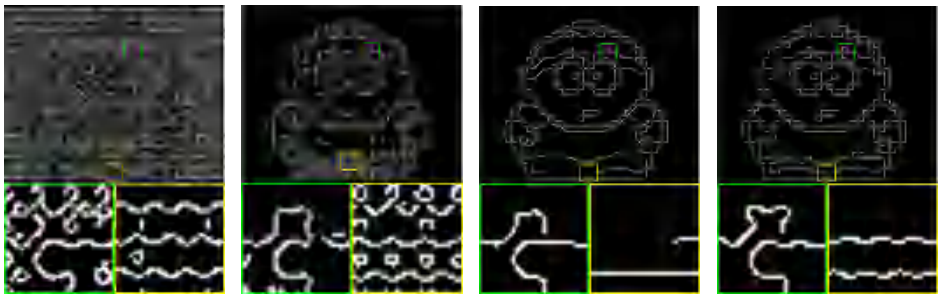

(e) Edge of (a) (f) Edge of (b) (g) Edge of (c) (h) Edge of (d)

FIGURE 9. The results of edge extraction. (a)-(d) are the results of different methods. (e)-(d) are obtained by a Canny edge detector. For each smoothed result, the zoomed-in patches of the smoothed output are shown at the bottom.

(a) Input (b) RTV [41] (c) L_0 [39] (d) SSTF [29]

(e) GFES [38] (f) TGHF [19] (g) NRCS [46] (h) Ours

FIGURE 10. Visual results of clip-art compression artifact removal with different approaches.

where TP means the correct number of edge pixels, FP is the wrong number of edge pixels and FN indicates the number of undetected edge pixels. Here, we adopt the public dataset in [41] and the canny operator for testing.

Table 2 presents the measurement results of the confusion matrix. Since the canny operator detects almost all possible edges, only the canny operator can obtain

TABLE 2. Numerical results of edge detection.

Method	Canny	Canny+ L_0	Canny+ SD filter	Canny+ Our
Precision	24.05%	70.30%	83.65%	**84.85**%
Recall	**21.91**%	15.58%	9.41%	16.73%
F-measure	20.04%	23.59%	16.43%	**27.54**%

the highest *Recall*. In addition, in terms of *Precision* and *F-score*, our method greatly improves the edge detection ability of the canny operator and is superior to the other two methods. Further, Figure 9 demonstrates the visual results of edge extraction with different methods. The L_0 cannot remove most of the textures in the image, while the SD filter ignores the details of this image. On the contrary, the edge extraction results generated after preprocessing by our method contain more structural details.

4.2.3. Clip-Art Compression Artifact Removal. The cartoon/clip-art compression artifact removal is also an important application of image smoothing. The traditional JPEG compression technology makes it difficult to balance the image quality and space, which leads to artifacts and affects the visual effect. This task requires us to smooth undesirable artifacts while preserving the overall structure of the image. Based on this, we can solve it well with our proposed method. Figure 10 demonstrates the artifact removal effect of different methods. It can be observed that the artifacts of L_0, GFES, and TGHF are not completely removed, and there are still obvious artifacts in the enlarged area. On the contrary, although RTV, SSTF, and NRCS have removed the artifacts, the edge processing of the details is not in place, resulting in blurring. In contrast, our proposed method performs better in removing artifacts and protecting weak edges.

To facilitate quantitative comparison, four high-quality original images were selected and nine JPEG-compressed images were generated for each original image. The quality factors for the nine compressed images were 10, 20, , and 90, respectively. A total of 36 JPEG compressed images with varying quality factors can be generated for the four original images. Nine distinct image smoothing techniques were employed to eliminate artifacts from the JPEG-compressed images, and the image quality was evaluated using PSNR and SSIM values. Table 3 illustrates the mean PSNR and SSIM values for the four images at varying quality factors, with the optimal outcomes highlighted in bold. As evidenced by the data presented in the table, our method demonstrably outperforms the other compared methods in terms of image quality.

4.2.4. Image Denoising. Image smoothing can become an effective tool in image denoising. By smoothing the image with a given noise level, a clean image without noise and containing the main structure can be obtained. Here, we compare the denoising performance of the model under different noise levels in Figure 11 and Figure 12. The classical L_0 method yields some residual noise. The PNLS and NRCS methods blur the edges. The result of our method is closer to the clean input image. In addition, from the numerical point of view, our method achieves the highest PSNR values under the two noise levels.

4.2.5. Image Abstraction. Image abstraction is to simplify image content and retain or even emphasize its important sensory characteristics. Most of this task is

TABLE 3. Quantitative comparison results (PSNR and SSIM) of clip-art compression artifact removal.

PSNR										
Quality	10	20	30	40	50	60	70	80	90	Ave.
L_0[39]	29.77	30.87	32.18	32.65	33.10	33.45	33.84	34.36	**34.96**	32.80
RTV[41]	29.95	31.12	32.25	32.75	33.06	33.46	33.76	34.28	34.71	32.82
RGF[44]	29.66	30.65	31.34	31.60	31.69	31.86	31.93	32.06	32.17	31.44
SSTF[29]	29.50	30.25	30.81	31.00	31.10	31.22	31.28	31.40	31.48	30.89
GFES[21]	29.65	30.83	31.61	32.08	32.19	32.45	32.65	32.94	33.07	31.94
LF[19]	29.27	30.55	30.99	31.48	31.81	32.08	32.46	32.99	33.38	31.67
NRCS[46]	29.66	30.80	31.69	32.12	32.42	32.71	32.99	33.42	33.80	32.18
Ours	**30.14**	**31.13**	**32.41**	**32.91**	**33.25**	**33.63**	**33.92**	**34.39**	34.94	**32.97**
SSIM										
Quality	10	20	30	40	50	60	70	80	90	Ave.
L_0[39]	0.9605	0.9597	0.9624	0.9622	0.9630	0.9629	0.9637	0.9654	0.9687	0.9632
RTV[41]	0.9691	0.9740	0.9772	0.9780	0.9799	0.9809	0.9811	0.9834	0.9853	0.9787
RGF[44]	0.9684	0.9746	0.9773	0.9777	0.9794	0.9802	0.9802	0.9820	0.9836	0.9781
SSTF[29]	0.9692	0.9739	0.9761	0.9763	0.9779	0.9786	0.9784	0.9801	0.9815	0.9769
GFES[21]	**0.9702**	0.9790	0.9811	0.9812	0.9830	0.9832	0.9828	0.9845	0.9848	0.9811
LF[19]	0.9645	0.9729	0.9765	0.9791	0.9808	0.9836	0.9854	0.9882	0.9895	0.9800
NRCS[46]	0.9648	0.9711	0.9738	0.9744	0.9761	0.9766	0.9873	0.9885	0.9899	0.9780
Ours	0.9701	**0.9798**	**0.9845**	**0.9857**	**0.9877**	**0.9887**	**0.9888**	**0.9902**	**0.9908**	**0.9851**

(a) Input (b) Noisy input(PSNR:20.64) (c) L_0 [39](PSNR:25.91)

(d) PNLS [38](PSNR:25.42) (e) NRCS [46](PSNR:27.15) (f) Ours(PSNR:27.64)

FIGURE 11. Denoising performance by different smoothing approaches.

to create new digital art forms, make images easier to understand, and can also be used as preprocessing for transforming into other art styles (such as pencil drawing and watercolor). This task has two main tasks: extract the edge of the image by Gaussian filtering after bilateral filtering. The obtained image has certain regional visual specificity and can be directly applied to edge detection. We perform image abstraction by replacing bilateral filtering with our method. Figure 13 shows the results of image abstraction. We can see that our results significantly enhance the edge, and the visual effect is pleasant. Our result can make the image easy to understand and helpful for subsequent artistic creation.

4.3. Parameter analysis. The regularization parameter λ is crucial in our model since its selection has a direct impact on the smoothed results. For this reason, we design an adaptive regularization parameter method to estimate λ. To further verify

(a) Input (b) Noisy input(PSNR:23.57) (c) L_0 [39](PSNR:25.55)

(d) PNLS [38](PSNR:25.84) (e) NRCS [46](PSNR:27.87) (f) Ours(PSNR:29.61)

FIGURE 12. Denoising performance by different smoothing approaches.

(a) Input

(b) Abstracted Image

FIGURE 13. Image abstraction results of our method.

the effectiveness of our parameter adaptation method, we analyze the visual images of different pairs of images. Figure 14 shows the images when $\lambda = 0.01$, $\lambda = 0.02$, and $\lambda = 0.05$ and the proposed parameter adaptation method, respectively. It is worth noting that our adaptive strategy has achieved ideal results: eliminated texture, and obvious edges. Although the smoothing effect of Figure 14(c) and Figure 14(d) is relatively close, the edge of Figure 14(d) is clearer. This shows that the parameter obtained by the adaptive method is more appropriate.

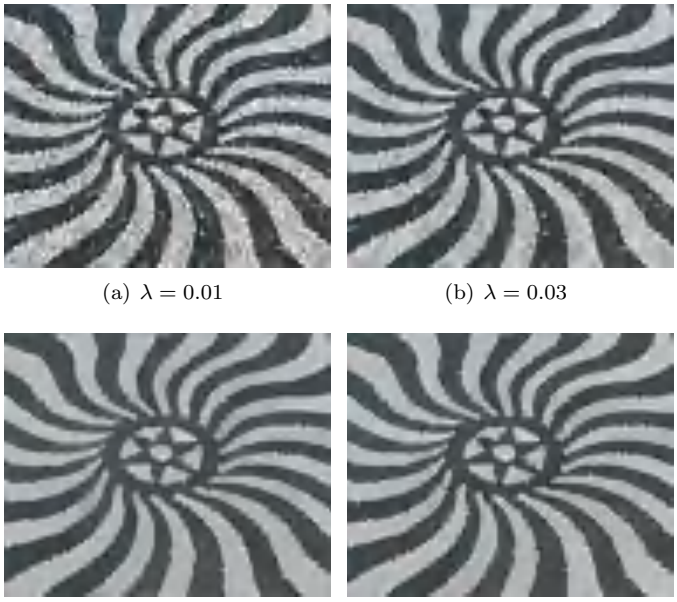

(a) $\lambda = 0.01$ (b) $\lambda = 0.03$

(c) $\lambda = 0.05$ (d) Parameter adaptation

FIGURE 14. Different λ values and adaptive parameter adjustment results.

5. Conclusion

In this paper, we explore a novel regularizer in the optimization framework to achieve texture smoothing of natural images. Our contributions were twofold. Firstly, we introduce a novel image smoothing model based on an adaptive weighted L_0 regularization to preserve weak edges. Unlike the classical L_0 regularization, we design a weighted matrix $\mathbf{T}$ to give different weights to different gradient directions. By selecting the appropriate weighted matrix, the model retains the main structure and enhances the ability to remove texture. Secondly, we apply the discrepancy principle to estimate the regularization parameter λ. The designed parameter selection scheme can adaptively select an appropriate parameter, reducing the inconvenience of the parameter adjustment process. In addition, we have also applied the new model to a variety of applications. Both quantitative and qualitative experiments show the advantages of our method.

Acknowledgements

This work was supported in part by NSFC (61971234, 12371518, 12171205, 12226003), Nanjing University of Posts and Telecommunications Project (NY223008), in part by Fundamental Research Funds for the Central Universities (2412023YQ006), and in part by the Postgraduate Research & Practice Innovation Program of Jiangsu Province (KYCX23_0958, SJCX23_0252).

References

[1] S. D. Babacan, R. Molina, and A. K. Katsaggelos, Variational bayesian blind deconvolution using a total variation prior, IEEE Transactions on Image Processing, 18 (2009), pp. 12–26.

[2] X. Cai, R. H. Chan, and T. Zeng, A two-stage image segmentation method using a convex variant of the mumford-shah model and thresholding, SIAM Journal on Imaging Sciences, 6 (2013), pp. 368–390.

[3] Q. Chen, J. Xu, and V. Koltun, Fast image processing with fully-convolutional networks, in IEEE International Conference on Computer Vision, 2017, pp. 2516–2525.
[4] C. Cho and S. Lee, Effective five directional partial derivatives-based image smoothing and a parallel structure design., IEEE Transactions on Image Processing, 254 (2016), pp. 1617–25.
[5] H. Cho, H. Lee, H. Kang, and S. Lee, Bilateral texture filtering, ACM Transactions on Graphics, 33 (2014), pp. 1–8.
[6] A. Conneau, H. Schwenk, L. Barrault, and Y. Lecun, Very deep convolutional networks for text classification, arXiv preprint arXiv:1606.01781, (2016).
[7] Q. Fan, J. Yang, D. Wipf, B. Chen, and X. Tong, Image smoothing via unsupervised learning, ACM Transactions on Graphics, 37 (2018), pp. 1–14.
[8] R. Fattal, M. Agrawala, and S. M. Rusinkiewicz, Multiscale shape and detail enhancement from multi-light image collections, ACM Transactions on Graphics, 26 (2007), pp. 1–9.
[9] Y. Feng, S. Deng, X. feng Yan, X. Yang, M. Wei, and L. Liu, Easy2hard: Learning to solve the intractables from a synthetic dataset for structure-preserving image smoothing, IEEE Transactions on Neural Networks and Learning Systems, 33 (2021), pp. 7223–7236.
[10] N. P. Galatsanos and A. K. Katsaggelos, Methods for choosing the regularization parameter and estimating the noise variance in image restoration and their relation, IEEE Transactions on Image Processing, 1 (1992), pp. 322–336.
[11] D. Geman and C. Yang, Nonlinear image recovery with half-quadratic regularization, IEEE Transactions on Image Processing, 4 (1995), pp. 932–946.
[12] B. Ham, M. Cho, and J. Ponce, Robust guided image filtering using nonconvex potentials, IEEE Transactions on Pattern Analysis and Machine Intelligence, 40 (2018), pp. 192–207.
[13] K. He, J. Sun, and X. Tang, Guided image filtering, IEEE Transactions on Pattern Analysis and Machine Intelligence, 35 (2012), pp. 1397–1409.
[14] K. He, X. Zhang, S. Ren, and J. Sun, Deep residual learning for image recognition, in IEEE Conference on Computer Vision and Pattern Recognition, 2015, pp. 770–778.
[15] L. He and Y. Wang, Image smoothing via truncated l_0 gradient regularisation, IET Image Processing, 12 (2018), pp. 226–234.
[16] L. He, Y. Xie, S. Xie, and Z. Chen, Structure-preserving texture smoothing via scale-aware bilateral total variation, IEEE Transactions on Circuits and Systems for Video Technology, 33 (2023), pp. 1493–1506.
[17] L. Karacan, E. Erdem, and A. Erdem, Structure-preserving image smoothing via region covariances, ACM Transactions on Graphics, 32 (2013), pp. 1–11.
[18] C. L. Lawson and R. J. Hanson, Solving least squares problems, in Classics in Applied Mathematics, 1976.
[19] F. Li and T. Li, A truncated generalized Huber prior for image smoothing, Applied Mathematical Modelling, 123 (2023), pp. 332–347.
[20] Q. Liu, C. Zhang, Q. Guo, and Y. Zhou, A nonlocal gradient concentration method for image smoothing, Computational Visual Media, 1 (2015), pp. 197–209.
[21] W. Liu, P. Zhang, Y. Lei, X. Huang, J. Yang, and M. K. Ng, A generalized framework for edge-preserving and structure-preserving image smoothing, IEEE Transactions on Pattern Analysis and Machine Intelligence, 44 (2021), pp. 6631–6648.
[22] Y. Liu, F. Zhang, Y. Zhang, X. Li, and C. Zhang, Image smoothing based on histogram equalized content-aware patches and direction-constrained sparse gradients, Signal Processing, 183 (2021), p. 108037.
[23] S. Mallat, A wavelet tour of signal processing, in Academic Press, Elsevier, 1998.
[24] H. Pan, Y. Wen, and H. Zhu, A regularization parameter selection model for total variation based image noise removal, Applied Mathematical Modelling, 68 (2019), pp. 353–367.
[25] Z. Pang, H. Zhang, S. Luo, and T. Zeng, Image denoising based on the adaptive weighted TVp regularization, Signal Processing, 167 (2020), p. 107325.
[26] Z. Pang, Y. Zhou, T. Wu, and D. Li, Image denoising via a new anisotropic total-variation-based model, Signal Processing: Image Communication, 74 (2019), pp. 140–152.
[27] S. Paris, S. W. Hasinoff, and J. Kautz, Local laplacian filters: edge-aware image processing with a laplacian pyramid, ACM Transactions on Graphics, 58 (2011), pp. 81–91.
[28] N. H. M. Rang and M. S. Brown, Fast and effective L0 gradient minimization by region fusion, in IEEE International Conference on Computer Vision, 2015, pp. 208–216.
[29] C. Song, C. Xiao, L. Lei, and H. Sui, Scaleadaptive structurepreserving texture filtering, Computer Graphics Forum, 38 (2019), pp. 149–158.

[30] X.-C. Tai and Y. Duan, Domain decomposition methods with graph cuts algorithms for image segmentation, International Journal of Numerical Analysis & Modeling, 8 (2011), pp. 137–155.
[31] A. Theljani, Non-standard fourth-order pde related to the image denoising multi-scale non-standard fourth-order pde in image denoising and its fixed point algorithm, International Journal of Numerical Analysis & Modeling, 18 (2021), pp. 38–61.
[32] G. Wang, T. Wong, and P.-A. Heng, Deringing cartoons by image analogies, ACM Transactions on Graphics, 25 (2006), pp. 1360–1379.
[33] W. Wang, N. Tian, and C. Wu, Two-phase image segmentation by nonconvex nonsmooth models with convergent alternating minimization algorithms, Journal of Computational Mathematics, 41 (2023), pp. 588–622.
[34] Y. Wen and R. H. Chan, Parameter selection for total-variation-based image restoration using discrepancy principle, IEEE Transactions on Image Processing, 21 (2012), pp. 1770–1781.
[35] Y. Wen, M. Zhao, and M. K. Ng, Cartoon and texture decomposition for color image in opponent color space, Applied Mathematics and Computation, 414 (2022), p. 126654.
[36] T. Wu, X. Gu, Y. Wang, and T. Zeng, Adaptive total variation based image segmentation with semi-proximal alternating minimization, Signal Processing, 183 (2021), p. 108017.
[37] T. Wu, C. Huang, Z. Jin, Z. Jia, and M. K. Ng, Total variation based pure quaternion dictionary learning method for color image denoising, International Journal of Numerical Analysis & Modeling, 19 (2022), pp. 709–738.
[38] J. Xu, Z. Liu, Y. Hou, X. Zhen, L. Shao, and M. Cheng, Pixel-level non-local image smoothing with objective evaluation, IEEE Transactions on Multimedia, 23 (2020), pp. 4065–4078.
[39] L. Xu, C. Lu, Y. Xu, and J. Jia, Image smoothing via L_0 gradient minimization, in Proceedings of the 2011 SIGGRAPH Asia conference, 2011, pp. 1–12.
[40] L. Xu, J. Ren, Q. Yan, R. Liao, and J. Jia, Deep edge-aware filters, in International Conference on Machine Learning, 2015, pp. 1669–1678.
[41] L. Xu, Q. Yan, Y. Xia, and J. Jia, Structure extraction from texture via relative total variation, ACM Transactions on Graphics, 31 (2012), pp. 1–10.
[42] F. Zhang, L. Dai, S. Xiang, and X. Zhang, Segment graph based image filtering: Fast structure-preserving smoothing, in IEEE International Conference on Computer Vision, 2015, pp. 361–369.
[43] H. Zhang and Y. Wang, Edge adaptive directional total variation, The Journal of Engineering, 2013 (2013), pp. 61–62.
[44] Q. Zhang, X. Shen, L. Xu, and J. Jia, Rolling guidance filter, European Conference on Computer Vision, (2014), pp. 815–830.
[45] F. Zhu, Z. Liang, X. Jia, L. Zhang, and Y. Yu, A benchmark for edge-preserving image smoothing, IEEE Transactions on Image Processing, 28 (2019), pp. 3556–3570.
[46] G. Zhu, X. Lv, L. Jiang, X. Sun, and B. Fang, Nonconvex regularization for convex image smoothing, Signal Processing, 205 (2023), p. 108862.

School of Science, Nanjing University of Posts and Telecommunications, Nanjing, 210023, China
E-mail: 1022082116@njupt.edu.cn
E-mail: wutt@njupt.edu.cn
E-mail: 1221087302@njupt.edu.cn
E-mail: 1220086613@njupt.edu.cn

School of Science, Jiangsu Ocean University, Lianyungang, 222005, China
E-mail: xiaoguanglv@jou.edu.cn

School of Information Engineering, Zhejiang Ocean University, Zhoushan, 3160220, China
E-mail: 2022048@zjou.edu.cn

School of Mathematics and Statistics, Northeast Normal University, Changchun, 130024, China
E-mail: liuj292@nenu.edu.cn